Redox Biology 80 (2025) 103503

Contents lists available at ScienceDirect

Redox Biology

journal homepage: www.elsevier.com/locate/redox

Metabolic dependency mapping identifies Peroxiredoxin 1 as a driver of resistance to ATM inhibition

Haojian Li [a,b,1], Takashi Furusawa [a,1], Renzo Cavero [a], Yunjie Xiao [a], Raj Chari [c], Xiaolin Wu [d], David Sun [d], Oliver Hartmann [e], Anjali Dhall [a], Ronald Holewinski [h], Thorkell Andresson [h], Baktiar Karim [i], Marina Villamor-Payà [f], Devorah Gallardo [j], Chi-Ping Day [g], Lipika R. Pal [g], Nishanth Ulhas Nair [g], Eytan Ruppin [g], Mirit I. Aladjem [a], Yves Pommier [a], Markus E. Diefenbacher [e], Jung Mi Lim [k], Rodney L. Levine [k], Travis H. Stracker [f], Urbain Weyemi [a,*]

[a] Developmental Therapeutics Branch, Center for Cancer Research, National Cancer Institute/National Institutes of Health, 37 Convent Drive, Bethesda, MD, 20892, USA
[b] Department of Molecular Biosciences, The University of Texas at Austin, Austin, TX, 78712, USA
[c] Genome Modification Core, Laboratory Animal Sciences Program, Frederick, MD, USA
[d] NCI Genomics Technology Laboratory, Cancer Research Technology Program, Frederick National Laboratory for Cancer Research/ Frederick, Maryland, USA
[e] Comprehensive Pneumology Center (CPC)/Institute of Lung Health and Immunity (LHI), Helmholtz Munich, Member of the German Center for Lung Research (DZL/CPC-M), Munich, Germany
[f] Radiation Oncology Branch/CCR/NCI, USA
[g] Cancer Data Science Lab/ Center for Cancer Research/National Cancer Institute/National Institutes of Health, Bethesda, MD, 20892, USA
[h] Protein Characterization Laboratory/Cancer Research Technology Program/Frederick National Laboratory for Cancer Research, Frederick, MD, USA
[i] Molecular Histopathology Laboratory/ Cancer Research Technology Program/Frederick National Laboratory for Cancer Research/ Frederick, Maryland, USA
[j] Laboratory Animal Sciences Program, Leidos Biomedical Research, National Cancer Institute, National Institutes of Health, Bethesda, MD, USA
[k] Laboratory of Biochemistry, National Heart, Lung, and Blood Institute, Bethesda, MD, USA

ARTICLE INFO

Keywords:
ATM kinase
Peroxiredoxin 1
Disulfide stress
p53 activation
RPL32 redox modification

ABSTRACT

Metabolic pathways fuel tumor progression and resistance to stress conditions including chemotherapeutic drugs, such as DNA damage response (DDR) inhibitors. Yet, significant gaps persist in how metabolic pathways confer resistance to DDR inhibition in cancer cells. Here, we employed a metabolism-focused CRISPR knockout screen and identified genetic vulnerabilities to DDR inhibitors. We unveiled Peroxiredoxin 1 (PRDX1) as a synthetic lethality partner with Ataxia Telangiectasia Mutated (ATM) kinase. Tumor cells depleted of PRDX1 displayed heightened sensitivity to ATM inhibition *in vitro* and in mice in a manner dependent on p53 status. Mechanistically, we discovered that the ribosomal protein RPL32 undergoes redox modification on active cysteine residues 91 and 96 upon ATM inhibition, promoting p53 stability and altered cell fitness. Our findings reveal a new pathway whereby RPL32 senses stress and induces p53 activation impairing tumor cell survival.

1. Introduction

In response to many types of DNA lesions, mammalian cells initiate a DNA damage response (DDR) to coordinate cell cycle progression, DNA repair and cell fate decisions to promote genome integrity [1–3]. DNA double-strand breaks (DSBs) are a particularly deleterious lesion that can lead to cell death and oncogenic chromosome translocations. DSBs are sensed by the MRN (MRE11-RAD50-NBS1) complex that activates the Ataxia-Telangiectasia mutated (ATM) kinase, a central transducer of the DDR in response to DSBs [4]. ATM phosphorylates a variety of proteins, including additional kinases and DNA repair proteins, to control cell signaling and fate after DNA damage. Loss of ATM kinase activity compromises the DDR and underlies the autosomal recessive disease, ataxia-telangiectasia (A-T). A-T patients exhibit pleiotropic symptoms that include immunodeficiency and elevated tumor predisposition [5]. ATM is crucial for maintaining genomic integrity. It is also

* Corresponding author. Developmental Therapeutics Branch National Cancer Institute, National Institutes of Health 37 Convent Drive, Bethesda, MD, 20892, USA.
E-mail address: urbain.weyemi@nih.gov (U. Weyemi).
[1] These authors contributed equally to this study.

https://doi.org/10.1016/j.redox.2025.103503
Received 26 August 2024; Received in revised form 12 December 2024; Accepted 15 January 2025
Available online 19 January 2025

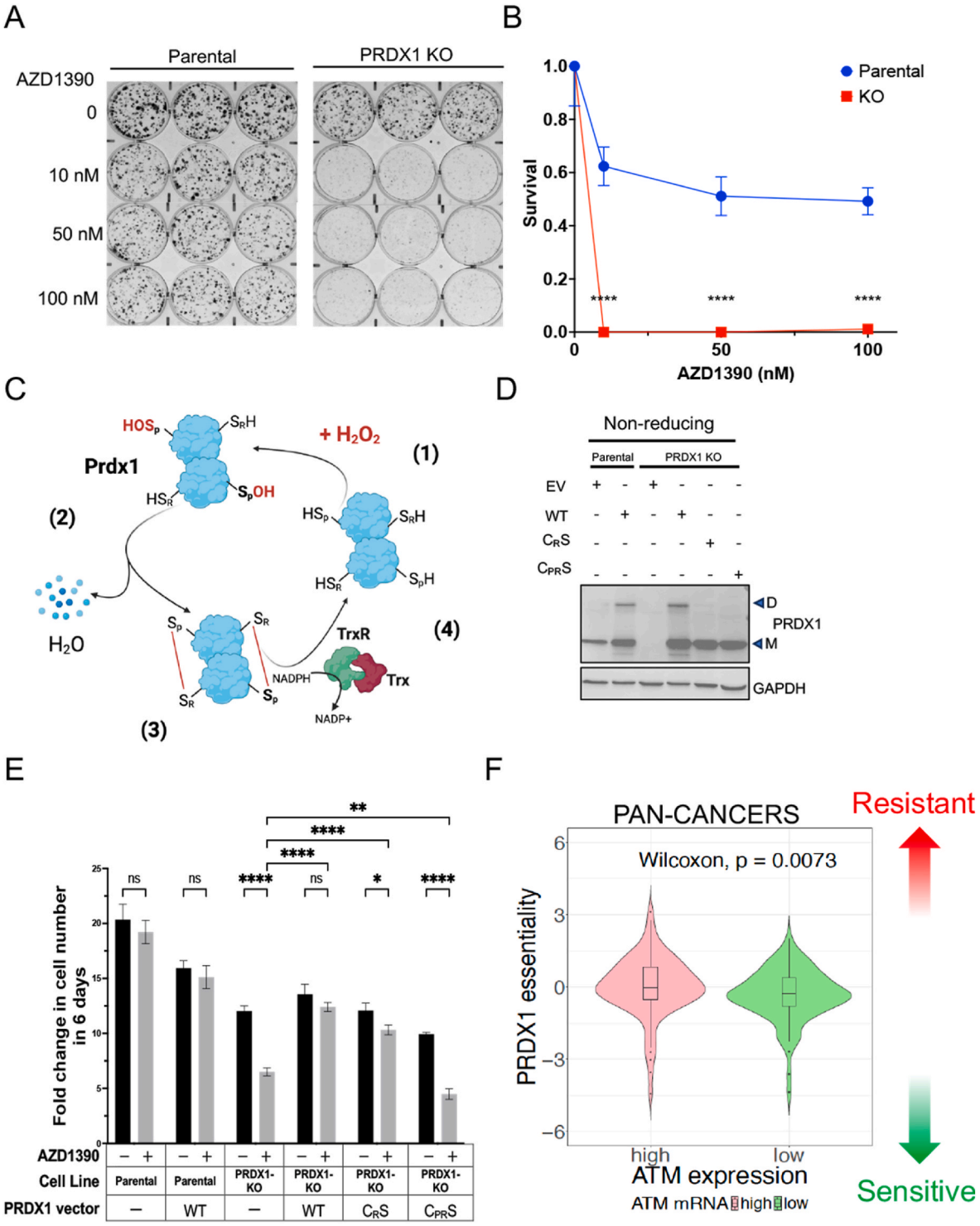

(caption on next page)

Fig. 1. Metabolism-focused CRISPR knockout screen identified PRDX1 as a critical driver for ATM inhibitor resistance. (A) Cells were treated for 10 days with the ATM inhibitor AZD1390 at lower concentrations (10, 50, 100 nM), and stained for colonies count. B. Quantification. (C) Diagram illustrating the redox cycle mediated by PRDX1 upon oxidative stress induced by hydrogen peroxide (H_2O_2). Two PRDX1 proteins act cooperatively as a dimer upon oxidation. PRDX1 contains a conserved cysteine residue (Cys 52) in its N-terminal region, known as peroxidatic Cys (C_p-SH) which senses H_2O_2 and undergoes oxidation forming a sulfenic acid (Step 1). Similar to other typical 2-Cys peroxiredoxins, PRDX1 contains an additional conserved Cys residue in its C-terminus (Cys 173) known as resolving Cys (C_R-SH). The disulfide structure formation in response to H_2O_2 consists of the peroxidatic Cys52 residue (C_P–OH) from one PRDX1 and the resolving Cys172 residue (C_RH) from the other homodimer subunit, and the release of H_2O (Steps 2 and 3). This disulfide bond structure can be readily reduced by the Thioredoxin (Trx)-Thioredoxin reductase (TrxR) complex using NADPH (Step 4). (D) Western blot of parental and PRDX1-knockout A549 cells infected with either empty vector (EV), wild-type PRDX1 (WT), or the resolving Cys172 mutant (C_RS), or the double mutant for peroxidatic Cys 52 and resolving Cys172 (C_{PR}S). Note PRDX1 dimer (D) formation in cells expressing the wild-type form of PRDX1, and the presence of PRDX1 monomer (M) in mutants. (E) Survival of A549 parental cells expressing empty vector (parental-EV), parental cells with wild-type PRDX1 (Parental-WT), and PRDX1 knockout cells expressing either empty vector (KO-EV), or PRDX1 mutants (KO-C_RS, KO-C_{PR}S). Cells were treated with AZD1390 (1 μM) for 6 days. (F) Relationship between *PRDX1* gene essentiality and ATM expression levels across pan-cancer cell lines. From the pan-cancer datasets, cancer cells were divided into two groups based on ATM expression levels: high ATM expression group (ATM mRNA high, represented by pink column on the left) and low ATM expression group (ATM mRNA low, represented by green column on the right). The y-axis represents the essentiality of PRDX1, which is the normalized growth reduction resulting from gene inactivation. Note that the essentiality of PRDX1 is significantly higher in high ATM-expressing cancer cells (pink) compared to low ATM-expressing cancer cells (green). Data are represented as mean ± SD; $n = 4$. ns, nonsignificant, $^{*}p < 0.05$; $^{**}p < 0.01$; $^{***}p < 0.001$; $^{****}p < 0.0001$.

a well-established tumor suppressor where high frequencies of mutations in ATM (or loss of ATM) are expressed in many cancer types. Loss of ATM function sensitizes cancer cells to the inhibition of alternative DDR pathways that ATM-deficient cells rely on for survival. ATM-deficient cancer cells also exhibit synthetic lethality with inhibition of Poly(ADP)Ribose-Polymerase (PARP) or ATR, as PARP-1 and the ATR kinase are respectively essential for SSB repair and the response to replication stress [6]. Three ATM inhibitors (AZD0156, AZD1390, and M3541) are currently in clinical trials for various cancers, potentially offering avenues for combination treatments based on synthetic lethality.

Of the many DDR proteins, ATM stands as one of the few whose function primarily links to the control of metabolism. ATM-deficient cells have increased reactive oxygen species (ROS), indicative of mitochondrial dysfunction [7], and ATM promotes the oxidative pentose phosphate pathway and regulates peroxisome turnover through pexophagy [8]. ATM activation leads to mitochondrial biogenesis and controls redox homeostasis in cancer cells by sustaining the NADPH pool, particularly in conditions of NRF2 activation and cysteine uptake [4,9–16]. However, significant gaps remain in understanding how ATM kinase coordinates redox homeostasis with the DDR when cancer cells are exposed to DDR-targeting drugs.

To establish a global map of synthetic lethal interactions between metabolic pathways and the DDR in cancer, we mined the *DepMap* database to identify metabolic genes whose loss may sensitize to silencing or depletion of the most prominent and druggable DNA repair kinases (ATM, ATR, WEE1, and DNA-PKcs). Using the focused CRISPR screen in cells treated with inhibitors of ATM, ATR, WEE1, and DNA-PKcs, we identified the metabolic determinants of DDR inhibitor resistance. We identified the major redox player Peroxiredoxin 1 (PRDX1), a key enzyme known for scavenging elevated peroxides via its active-site peroxidative cysteine, as a driver of resistance to ATM inhibitors, both *in vitro* and in mouse models. Mapping the proteome of thiol oxidation via a double alkylation assay, we unveiled a novel signaling pathway mediated by disulfide stress-dependent p53 activation, which involves changes in the redox status of the ribosomal protein RPL32.

2. Results and discussion

2.1. Peroxiredoxin 1 loss sensitizes lung cancer cells to ATM inhibition

To comprehensively investigate the interplay between cellular metabolism and the global DDR in cancer cells, we established a gene dependency network, focusing on non-small cell lung cancer (NSCLC) cell lines to minimize lineage effects. Leveraging the *DepMap* database, we curated a list of metabolic genes exhibiting a positive correlation with the key druggable DNA repair kinases ATM, ATR, WEE1, and DNA-PK when comparing their expression and essentiality data using non-small cell lung cancer lines to minimize lineage effects. Of the ~3000 human metabolic genes analyzed [17], only 407 exhibited a significant positive correlation with the gene effect of ATM, ATR, WEE1, and DNA-PK (Table S1). We established a focused CRISPR knockout library with the 407 genes and performed an essentiality screen in the non-small cell lung cancer cell line A549 treated with inhibitors for ATM, ATR, WEE1, and DNA-PKcs (Fig. S1A). The A549 cells are KEAP1 mutant serving as a suitable model for highly metabolic and redox stress sensitive lines. We used the *MAGECKFlute* pipeline to assess changes in sgRNA guide abundance [18] (Fig. S1A) and identified clusters of metabolic genes whose loss sensitized lung cancer cells to DDR inhibitors (Figs. S1B and C, and Table S2).

The newly established DDR-metabolism dependency map was substantiated by the identification of *PTEN*, a tumor suppressor gene well-established for its synthetic lethal interaction with ATM loss (Fig. S1C) [19,20]. In the same cluster as PTEN was Peroxiredoxin 1 (PRDX1), a key regulator of redox reactions that was not previously linked to ATM signaling (Fig. S1C). We validated Peroxiredoxin 1 (PRDX1) as a major driver of resistance to the ATM inhibitor AZD1390 (Fig. 1A–and B), and to a lesser extent, to the ATR inhibitor VE-821, by comparing the responses of PRDX1 knockout and wildtype cells (Figs. S1D–G). In contrast, the DNA-PK inhibitor NU7441 failed to selectively sensitize PRDX1-deficient cells to death (Fig. S1H). These findings demonstrated that PRDX1 loss sensitizes non-small cell lung cancer cells A549 to ATM inhibition and support the robustness of our DDR-metabolism dependency map.

PRDX1 belongs to a family of cysteine-dependent peroxidases that reduce hydrogen peroxide (H_2O_2) or alkyl peroxide (ROOH) via a conserved cysteine residue (Cys 52) in its N-terminal region, known as peroxidatic Cys (C_p-SH) [21–27]. Similar to other typical 2-Cys peroxiredoxins, PRDX1 contains an additional conserved Cys residue in its C-terminus (Cys 173) known as resolving Cys (C_R-SH). The disulfide structure formation in response to H_2O_2 consists of the peroxidatic Cys52 residue (C_P–OH) from one PRDX1 and the resolving Cys172 residue (C_RH) from the other homodimer subunit. This disulfide structure can be readily reduced by the Thioredoxin (Trx)-Thioredoxin reductase (TrxR) complex and NADPH [21,28–30] (Fig. 1C). Mutation of both the peroxidatic Cys 52 and resolving Cys172 residues in PRDX1 impairs disulfide structure formation and its peroxidatic activity (Fig. 1D). To elucidate the extent to which Cys residues of PRDX1 control response to ATM inhibition, we analyzed cell survival upon AZD1390 treatment. While ectopic expression of wild-type PRDX1 or a PRDX1 Cys172 mutant in PRDX1 knockout cells restored the resistance to AZD1390 treatment, mutation of both C_p-SH and C_R-SH (Cys52/Cys172) of PRDX1 did not rescue sensitivity to ATM inhibitor (Fig. 1E). These observations suggest that the peroxidatic activity of PRDX1 is required for resistance to ATM inhibitors. We investigated whether the single deletion of PRDX1 could trigger compensatory upregulation of other typical 2-Cys

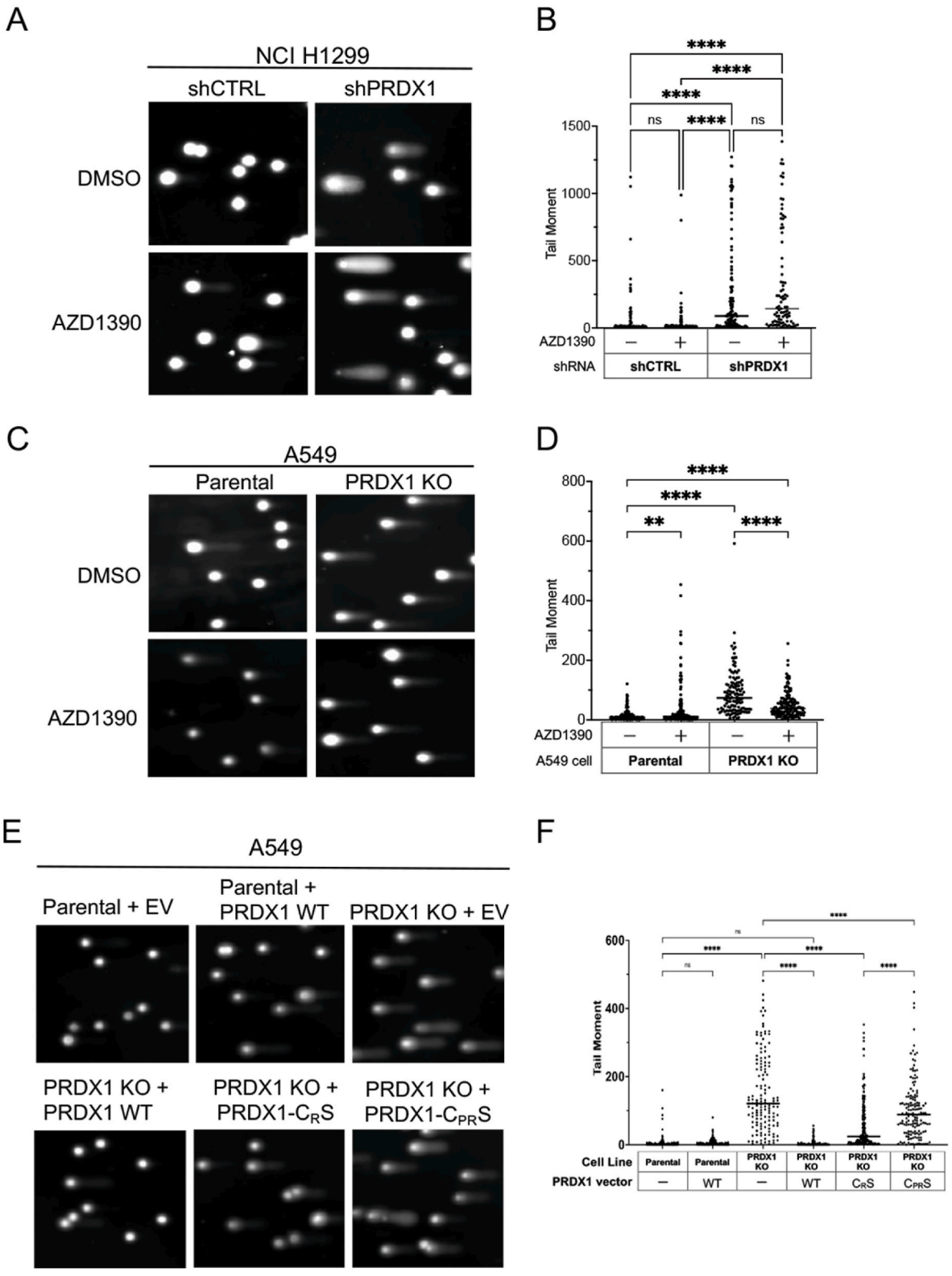

Fig. 2. PRDX1 loss promotes DNA breaks in NSCLC lines. (A) NCIH1299 Shcontrol and shPRDX1 cells were treated with DMSO or AZD1390 at a dose of 1 μM for 6 days. (B) Quantification of panel A. One-way ANOVA followed by Tukey's multiple comparisons test. (C) A549-Cas9 parental and PRDX1 KO cells were treated with DMSO or with AZD1390 at 1 μM for 6 days. (D) Quantification of panel C. One-way ANOVA followed by Tukey's multiple comparisons test. (E) A549-Cas9 parental and PRDX1 KO cells were infected with empty vector (EV), PRDX1 wild type (WT), PRDX1-C_RS, or PRDX1-$C_{PR}S$ plasmids and used for comet assay. (F) Quantification of panel E. One-way ANOVA followed by Tukey's multiple comparisons test. ns, nonsignificant, *$p < 0.05$; **$p < 0.01$; ***$p < 0.001$; ****$p < 0.0001$.

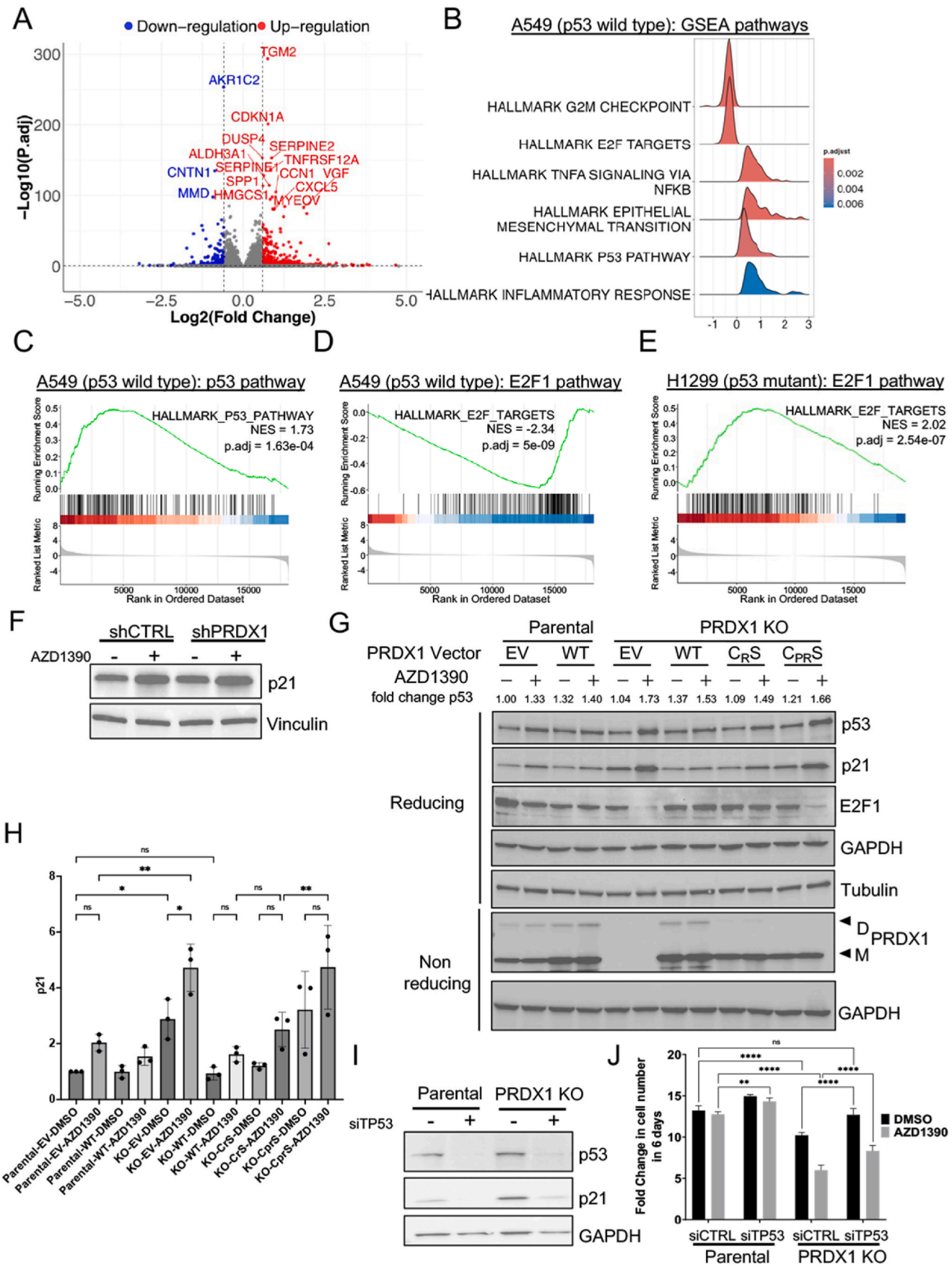

(caption on next page)

Fig. 3. p53 activation impaired growth in PRDX1-deficient cells in response to ATM inhibition. (A) Volcano plot representing gene expression profile of sgRNA-PRDX1 infected-A549-Cas9 cells (sgPRDX1) treated or not (DMSO) with AZD1390 (1 μM) or DMSO for 6 days. Blue dots represent the most downregulated genes, and red dots represent the most upregulated genes in PRDX1-deficient cells treated with AZD1390. (B) Ridgeplot of Gene Set Enrichment Analysis (GSEA) using Hallmark gene sets by comparing sgRNA-PRDX1 infected-A549-Cas9 cells (sgPRDX1) treated AZD1390 (1 μM) or DMSO. (C) Gene Set Enrichment Analysis (GSEA) of RNA-seq positively enriched genes related to p53 activation pathways corresponding to the samples A549-sgPRDX1 treated with AZD1390. (D) GSEA of RNA-seq negatively enriched genes related to E2F1 activation pathways corresponding to the samples A549-sgPRDX1 treated with AZD1390. (E) GSEA of RNA-seq positively enriched genes related to E2F1 activation pathways corresponding to the samples H1299-sgPRDX1 treated with AZD1390. (F) Western blot of control (shCTRL) and PRDX1-depleted NCI–H1299 cells (shPRDX1) treated with AZD1390 (1 μM) for 6 days. Note p21 expression level is unchanged between control and PRDX1-deficient cells treated with AZD1390. GAPDH was used as a loading control. (G) Western blot of parental (Parental) and PRDX1-knockout (PRDX1 KO) A549 cells infected with either empty vector (EV) or wild-type PRDX1 (WT), or with the resolving Cys172 mutant (C_RS), or the double mutant for peroxidatic Cys 52 and resolving Cys172 ($C_{PR}S$). Note PRDX1 dimer (D) formation in cells expressing the wild-type form of PRDX1, and the presence of PRDX1 monomer (M) in mutants using nonreducing conditions. Cells were treated with AZD1390 (1 μM) for 6 days. (H) Quantification of p21 protein levels as a direct indicator of p53 activation. (I) Western blot of parental A549 cells (parental) and PRDX1-knockout cells (PRDX1 KO) treated with AZD1390 (1 μM) for 6 days following p53 silencing by small interference RNA (siRNA). Note p53 expression level was detected as a direct readout of the siRNA efficacy over 6 days, and GAPDH was used as a loading control. P53 expression level was detected 48 h post siRNA transfection. (J) Survival of cells established in (I). ns, nonsignificant, $*p < 0.05$; $**p < 0.01$; $***p < 0.001$; $****p < 0.0001$.

peroxiredoxins. Our data revealed a marginal increase in PRDX4 expression in PRDX1-deficient cells, while the levels of PRDX2 and PRDX3 remained unchanged (Fig. S2). Interestingly, ATM inhibition also led to a slight increase in PRDX4 levels (Fig. S2). However, the extent to which this PRDX4 upregulation contributes to the observed phenotype in PRDX1 knockout cells remains unclear and warrants further investigation. Taken together, these results showed that the loss of PRDX1 peroxidatic activity is synthetic lethal with ATM kinase inhibition. PRDX1 was long studied for its essential roles in cell signaling [19], including transferring oxidative equivalents to target partners via redox relay [27,31] or protecting target partners from oxidation via the redox cycle [32,33]. Our findings established PRDX1 as a key driver of resistance to DDR inhibition.

To investigate whether the relationship between PRDX1 and ATM may be clinically relevant, we conducted an expression-level comparison of *PRDX1* and *ATM* in a large panel of human malignancies, including a cohort of solid tumors of diverse origins (pan-cancers cohort) from *The Cancer Genome Atlas* (*TCGA*) pan-cancer datasets. The transcript levels of *ATM* and *PRDX1* inversely correlated across a large panel of over 10,071 specimens from diverse origins (pan-cancers panel, $n = 10{,}071$, $r = -0.42$, $p < 2.2e^{-16}$) (Fig. S3, Part I-III). These observations collectively suggest that, at least in a subset of patients, PRDX1 and ATM may cooperate to inhibit cancer cell growth, providing unique clues that both genes may potentially be targeted to improve patient response.

To further validate the role of PRDX1 as a synthetic lethality partner of ATM, we tested the essentiality of PRDX1 based on ATM transcript levels across various cancer cell lines using the *SELECT* pipeline [34]. From the curated *in vitro* pan-cancer datasets [35, 36], we asked whether the growth suppression induced by knocking out/down or pharmacologically inhibiting ATM is stronger when PRDX1 is inactive using a one-sided *Wilcoxon rank-sum* test. As shown in Fig. 1F, the essentiality of PRDX1 was significantly higher in ATM-high cancer, suggesting that tumor cells with high ATM exhibit elevated resistance to PRDX1 deletion, whereas tumor cells with low ATM are more sensitive to PRDX1 loss (P-value = 0.0073, one-sided Wilcoxon test). A similar PRDX1 essentiality based on ATM transcripts levels was found across NSCLC lines (P-value = 0.013, one-sided Wilcoxon test) (Fig. S4A). We identified a similar synthetic lethal interaction between ATR and PRDX1 (Fig. S4B), whereas DNA-PKcs levels in tumors were not correlated with PRDX1 essentiality, consistent with our screening results (Fig. S4C). As essentiality analysis was performed using a pan-cancer dataset (270 tumor cell lines), these results suggest that the synthetic lethality between PRDX1 and ATM, and potentially ATR, extends beyond NSCLC. Altogether, we uncovered a novel synthetic lethal interaction between ATM and PRDX1 in tumor cells. This interaction is conserved across most cancer types, establishing PRDX1 as potentially a universal synthetic lethality partner with ATM.

2.2. Cell growth arrest induced by ATM inhibition in PRDX1-deficient cells is p53-dependent

While the role of ATM in orchestrating redox homeostasis and cell death has been extensively studied in the context of DDR and metabolism, it remained unclear why ATM inhibition was essential in the absence of PRDX1 [3,4,14,37–39]. Previous seminal reports linked PRDX1 to genome maintenance functions, including protecting telomeres from oxidation [40], safeguarding genomic integrity via protecting RAD51 from oxidation in response to exogenous stress [23], as well as maintaining nucleotide pool synthesis following exposure to replication stress inducers [41]. To determine if the impaired proliferation induced by ATM inhibition in PRDX1-deficient cells was caused by elevated DNA damage, we employed the Comet assay to quantify the total DNA break levels in two NSCLC lines, NCI–H1299 and A549. We observed that PRDX1 loss alone yielded significant levels of DNA breaks (Fig. 2A–D). However, ATM inhibition did not promote further DNA damage, suggesting that cell death following ATM inhibition in PRDX1-depleted cells is independent of effects on DNA repair pathways. To ascertain the importance of PRDX1 enzymatic activity in DNA damage, we analyzed levels of DNA breaks in A549 parental, PRDX1-knockout cells, and in PRDX1-knockout cells complemented with either PRDX1 wild type or enzymatic mutants. Ectopic expression of wild-type PRDX1 in the knockout cells fully mitigated DNA damage, while a PRDX1 mutant for resolving Cys172 partially reduced DNA damage (Fig. 2E and F). In contrast, mutation of both C_P-SH and C_R-SH (Cys52/Cys172) led to elevated DNA damage, similar to what was observed in PRDX1 knockout cells. These data indicate that PRDX1 depletion alone is sufficient to promote DNA damage in lung cancer cells and the synthetic lethal effects of ATM inhibiton are independent of futher defects in DNA repair.

To identify alternative pathways that may be influenced by ATM inhibition, we performed RNA-seq to identify differentially expressed genes between control cells or PRDX1-depleted cells after treatment with the ATM inhibitor AZD1390 for 6 days. We observed a significant shift in genes involved in cell cycle arrest, with CDKN1A (p21) emerging as one of the most prominently activated genes in PRDX1-depleted cells treated with ATM inhibitor (Fig. 3A). Employing *Gene Set Enrichment Analysis (GSEA)*, we identified the p53 response signature as one of the prominently activated pathways following ATM inhibition in PRDX1-deficient cells (Fig. 3B and C). These results were corroborated by marked repression of the transcriptional signature mediated by E2F transcription factors and their downstream targets, consistent with reduced S-phase entry (Fig. 3D). In contrast to the p53 wild-type A549 NSCLC line (Fig. 3D), ATM inhibition in p53-mutant NCI–H1299 cells was accompanied by an activation of the E2F-dependent pathway (Fig. 3E). Unlike the A549 NSCLC line, no further p21 activation was observed in PRDX1-deficient cells following ATM inhibition (Fig. 3F).

Next, we examined the direct impact of PRDX1 peroxidatic function

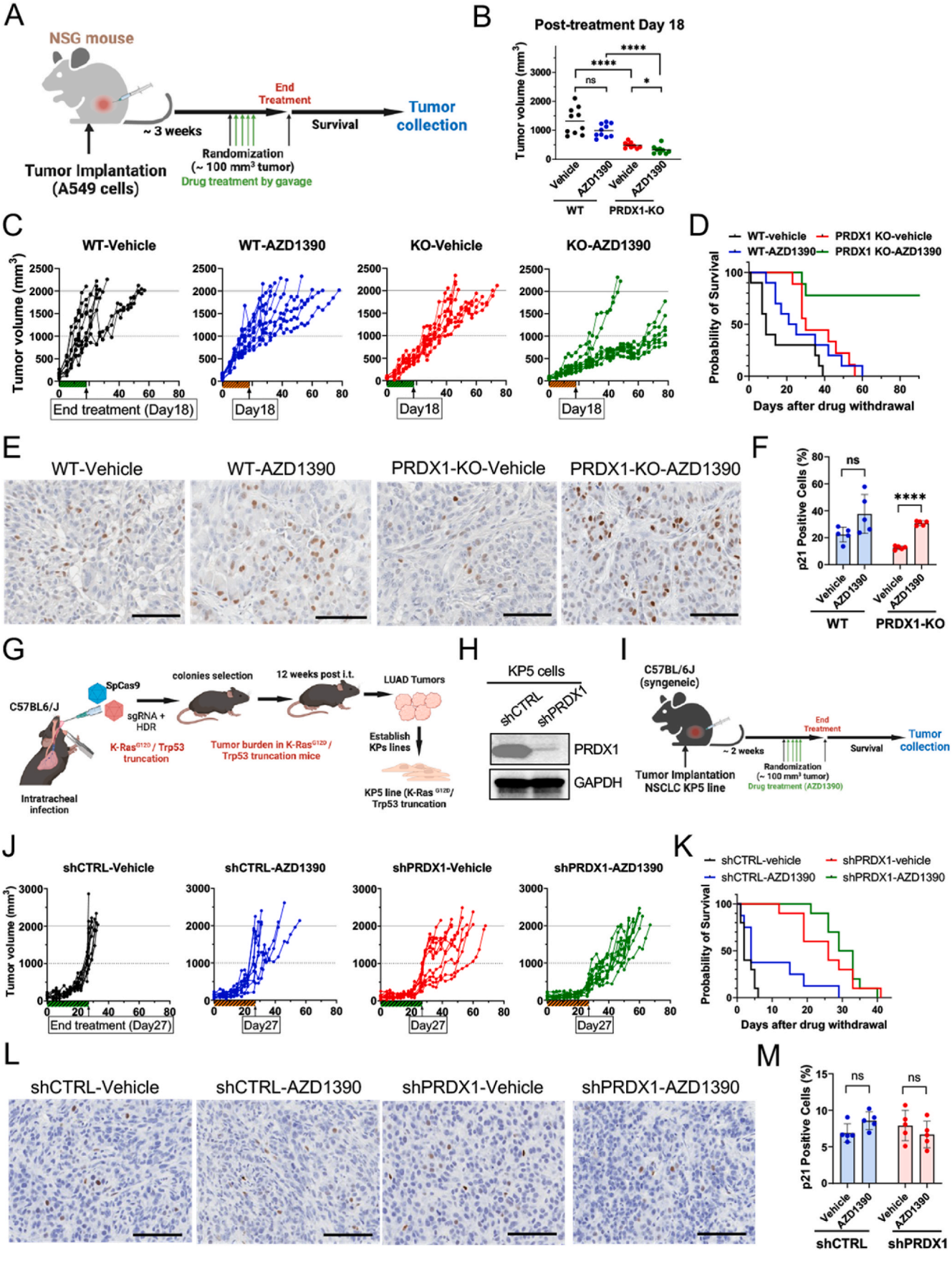

(caption on next page)

Fig. 4. p53 status dictates the response of Peroxiredoxin 1-deficient cells to ATM inhibitors *in vivo*. (A) Schematic of the experimental tumor model using A549 parental and PRDX1-knockout cells. (B) Quantification of tumor volume on Day 18 following treatment with AZD1390 (20 mg/kg). (C) Measurement of individual tumor volume throughout the experiment. (D) Kaplan-Meier survival curves for NSG mice injected with parental and PRDX1-KO cells and treated as indicated; $n = 10$. Statistical significance determined by log-rank test indicates. (E) Immunohistochemistry staining of p21-positive tumor cells (brown staining) comparing A549 parental and PRDX1-knockout cells treated with AZD1390 at the endpoint. (F) Quantification of p21-positive tumor cells. (G) Generation of KP5 tumor cells using CRISPR-mediated K-Ras mutation (G12D) and loss-of-function TP53 truncation, followed by intratracheal infection into C57BL/6J mouse and tumor burden. (H) Western blot of control (shCTRL) and PRDX1-depleted (shPRDX1) KP5 cells for the detection of PRDX1 expression level. (I) Schematic of the experimental tumor model using control (shCTRL) and PRDX1-depleted (shPRDX1) KP5 cells to establish a syngeneic model. (J) Measurement of individual tumor volume throughout the experiment. (K) Kaplan-Meier survival curves for C57BL/6J mice injected with control (shCTRL) or PRDX1-depleted (shPRDX1) KP5 cells and treated as indicated; $n = 10$. Statistical significance determined by log-rank test indicates. (L) Immunohistochemistry staining of p21-positive tumor cells (brown staining) comparing control (shCTRL) or PRDX1-depleted (shPRDX1) KP5 cells treated with AZD1390 at the endpoint. (M) Quantification of p21-positive tumor cells. ns, nonsignificant, $^{*}p < 0.05$; $^{**}p < 0.01$; $^{***}p < 0.001$; $^{****}p < 0.0001$. Note. Fig. 4A, G, and I are designed using *Biorender*.

on p53 pathway activation following ATM inhibition. We analyzed the expression of p53, p21 and E2F1 in A549 parental, PRDX1 knockout cells, and in PRDX1 knockout cells complemented with either PRDX1 wild type or enzymatic mutants (Fig. 3G). ATM inhibition in PRDX1-knockout cells resulted in elevated levels of p53 and p21 expression and reduced E2F1, an effect that was complemented by the expression of wild-type PRDX1 (Fig. 3G, and Fig. S5A). Expression of PRDX1-Cys172 (C_RS) also reduced p53 and p21 activation, albeit to a lesser extent than wild type, whereas PRDX1-Cys52/172 ($C_{PR}S$) phenocopied the knockout with elevated p53 and p21 and significant repression of E2F1 expression (Fig. 3G). These findings underscore the requirement of p53 accumulation and its activation in triggering cell growth arrest in PRDX1-deficient cells in response to ATM inhibition. Silencing of p53 using small interfering RNA (Fig. 3H) partially restores the proliferative ability in PRDX1-deficient cells, further supporting the pivotal role of p53 in mediating cell arrest upon ATM inhibition (Fig. 3I). Our results point to a mechanism of p53 activation in PRDX1-deficient cells treated with ATM inhibitors that contrasts with the canonical pathway of redox-dependent p53 activation, which involves phosphorylation of p53 by ATM [37,42]. Our findings indicate that ATM inhibition was not accompanied by a reduction in the phosphorylated pool of p53 (Ser15), nor that p53 accumulation is the result of MDM2 depletion, the most abundant p53 negative regulator (Fig. S5B). It remains unclear whether other regulators of p53 or specific posttranslational modifications of MDM2 are involved.

To determine whether p53 activation is associated with significant changes in cell cycle progression, we assessed cell cycle phases in both parental and PRDX1-deficient A549 cells following 6 days of ATM inhibition. While PRDX1 loss modestly impeded cell entry into S-phase, the combined effect of ATM inhibition and PRDX1 loss resulted in a substantial 36.55 % reduction in S-phase cells compared to untreated parental cells (Figs. S6A and B). This delay was further evidenced by pronounced alterations in cell morphology, as PRDX1-deficient cells display an enlarged and flattened phenotype following ATM inhibition (Fig. S6C). Conversely, ATM inhibition in p53-mutant NCI–H1299 cells did not hinder cells from entering S-phase (Figs. S6D and E). Unlike in A549 cells, ATM inhibition facilitated cell cycle progression upon PRDX1 loss in parallel to E2F1 pathway activation, reflecting the lack of p53-mediated arrest (Figs. S6D and E). Together, these findings underscore the pivotal role of p53 as a mediator of cell growth arrest induced by ATM inhibition in PRDX1-deficient cells.

2.3. p53 status dictates the response of Peroxiredoxin 1-deficient cells to ATM inhibitors in vivo, and the survival of patients across multiple human malignancies

To determine if PRDX1 loss conferred similar responses to ATM inhibitor treatment *in vivo*, we established xenografts using the human NSCLC line A549 (p53 wild type). Parental A549 and PRDX1 knockout tumors were implanted into immunocompromised *NSG* mice, followed by treatment with AZD1390 (Fig. 4A). We observed a significant ~63.5 % reduction ($p < 0.0001$) in tumor growth upon PRDX1 depletion at Day 18 post-treatment with AZD1390 compared to parental cells with vehicle treatment (Fig. 4B). Conversely, treatment with AZD1390 in mice injected with parental cells only showed a minimal response (25.3 % reduction, $p > 0.05$). PRDX1 loss further enhanced the sensitivity of A549 cells to ATM inhibitor treatment, resulting in an additional 32.7 % reduction in tumor growth ($p = 0.015$) (Fig. 4B).

To assess if ATM inhibition is essential to establish a durable response in PRDX1-deficient cells *in vivo*, drug treatment was discontinued on Day 18, and tumor growth was monitored for long-term overall survival. ATM inhibitor treatment of PRDX1 knockout xenografts led to a significant halt in tumor growth, and a prolonged inhibitory response (Fig. 4C), resulting in a twofold increase in overall survival for most animals post-dosing period (Fig. 4D). This prolonged response following ATM inhibition was accompanied by a durable increase in p53 activation, as evidenced by p21 accumulation in PRDX1-deficient tumor cells treated with ATM inhibitor (Fig. 4E and F).

To evaluate the relevance of p53 status in the response of PRDX1-deficient cells to ATM inhibitor, we employed KP5 cells, a murine lung adenocarcinoma syngeneic line with K-Ras mutation and p53 truncation [43] (Fig. 4G and H). Mice were subjected to gavage with AZD1390 for 4 weeks, followed by drug withdrawal and monitoring of tumor progression for an additional 5 weeks (Fig. 4I). Unlike in A549 cells, treatment of PRDX1-deficient KP5 xenografts with the ATM inhibitor failed to significantly yield a durable response, presumably due to the absence of p53-mediated arrest upon ATM inhibition (Fig. 4J). There was no significant difference in overall survival between the vehicle group and the AZD1390-treated group upon PRDX1 loss (Fig. 4K). These observations were supported by the lack of p21 accumulation in PRDX1-deficient tumors treated with the ATM inhibitor (Fig. 4L and M), suggesting the absence of p53 activation in response to ATM inhibition. These findings indicate that ATM inhibition induces tumor cell arrest in PRDX1-depleted cells specifically when tumor cells retain functional p53.

We next employed xenografts with the p53-mutant NSCLC line NCI–H1299 (Fig. 5A and B). Treatment of PRDX1-deficient NCI–H1299 xenografts with the ATM inhibitor did not yield a significant reduction in tumor growth, mirroring observations with the p53-truncated KP5 cells (Fig. 5C), confirming that there were no differential responses stemming from species and immune status of the models. These results align with the overall survival outcomes (Fig. 5D), demonstrating negligible differences in survival between mice inoculated with PRDX1-deficient cells treated with either vehicle or AZD1390. To evaluate whether the difference in tumor growth following ATM inhibition can be attributed to PRDX1 reactivation, we performed immunohistochemical staining to assess PRDX1 expression levels. As shown in Figs. S7A–C, PRDX1 levels remained diminished at the experiment's endpoint in PRDX1-deficient tumors.

To investigate the predictive value of p53 status in patients for overall survival, we analyzed a large panel of human malignancies from *TCGA* datasets. Patients with low expression of both *ATM* and *PRDX1* exhibit longer overall survival when p53 is functional (Fig. 6A–C, E, and G). However, the p53 status of the tumor becomes less relevant in patients with high expression of both *ATM* and *PRDX1* (Fig. 6B–D, F, and H). This indicated that tumors with lower *ATM* and *PRDX1* expression

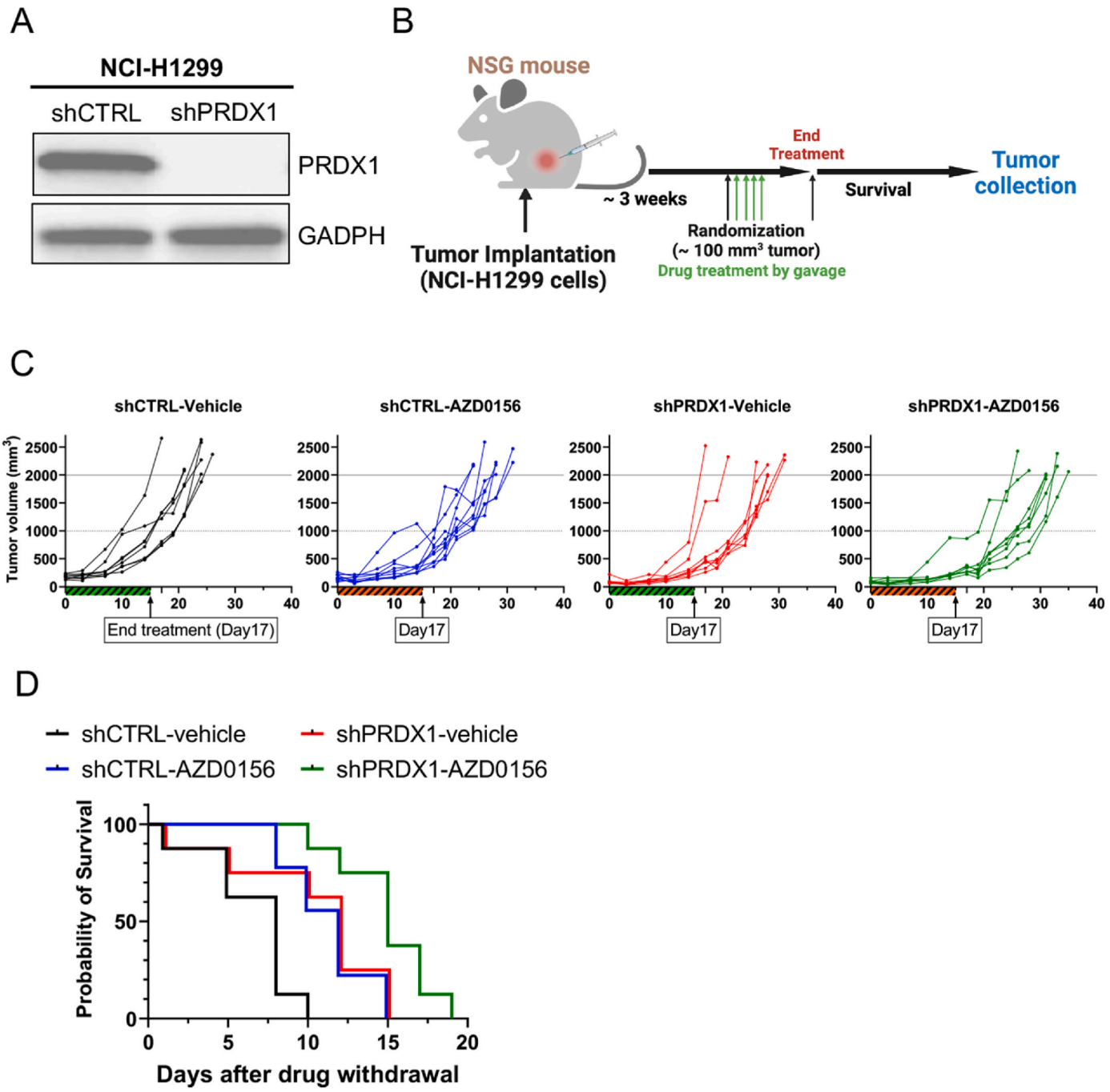

Fig. 5. Cells devoid of p53 activity are less sensitive to ATM inhibition upon PRDX1 loss. (A) Western blot analysis of NCIH1299 shControl and shPRDX1 cells. (B) Schematic of the experimental tumor model using NCIH1299 shControl (shCTRL) and shPRDX1 cells. (C) Measurement of individual tumor volume throughout the experiment. (D) Kaplan Meier survival curves for NSG mice injected with NCIH1299 shControl (shCTRL) and shPRDX1 cells and treated as indicated. n = 8–9. Statistical significance determined by log-rank test indicates. Note. Fig. 5B is designed with *BioRender*.

may show lower aggressiveness when p53 is functional, further substantiating findings in mice. Altogether, these findings provide evidence for stratifying patients with low expression of PRDX1 and functional p53 as likely responders to ATM inhibitors.

2.4. *RPL32 is oxidized upon ATM inhibition promoting p53 activation*

To determine what pathways may be involved in the reduced cell growth induced by ATM inhibition in PRDX1-depleted cells, we employed treatments with TCEP (inhibits cysteine disulfide bond formation and disulfide stress), Ferrostatin-1 (inhibits lipid peroxidation and ferroptosis), or Z-VAD-fmk (pan-caspase inhibitor that inhibits apoptosis). AZD1390 treatment reduced cell growth (Fig. 7A; 2nd vs. 1st black bar), and knockout of PRDX1 enhanced the efficacy of AZD1390 (the corresponding gray bars). Treatment with TCEP eliminated the efficacy of AZD1390 (6th vs. 2nd gray bar). Other agents were ineffective in preventing cell death induced by ATM inhibitors in PRDX1-depleted cells (Fig. 7A), suggesting that disulfide stress plays a pivotal role in the synthetic interaction. To this end, we analyzed ROS levels using *CellRox Green* and found that PRDX1 loss is accompanied by a slight increase in ROS levels (orange vs. red in Fig. 7B–and C), whereas ATM inhibition triggered a two-fold increase in ROS levels in PRDX1-deficient

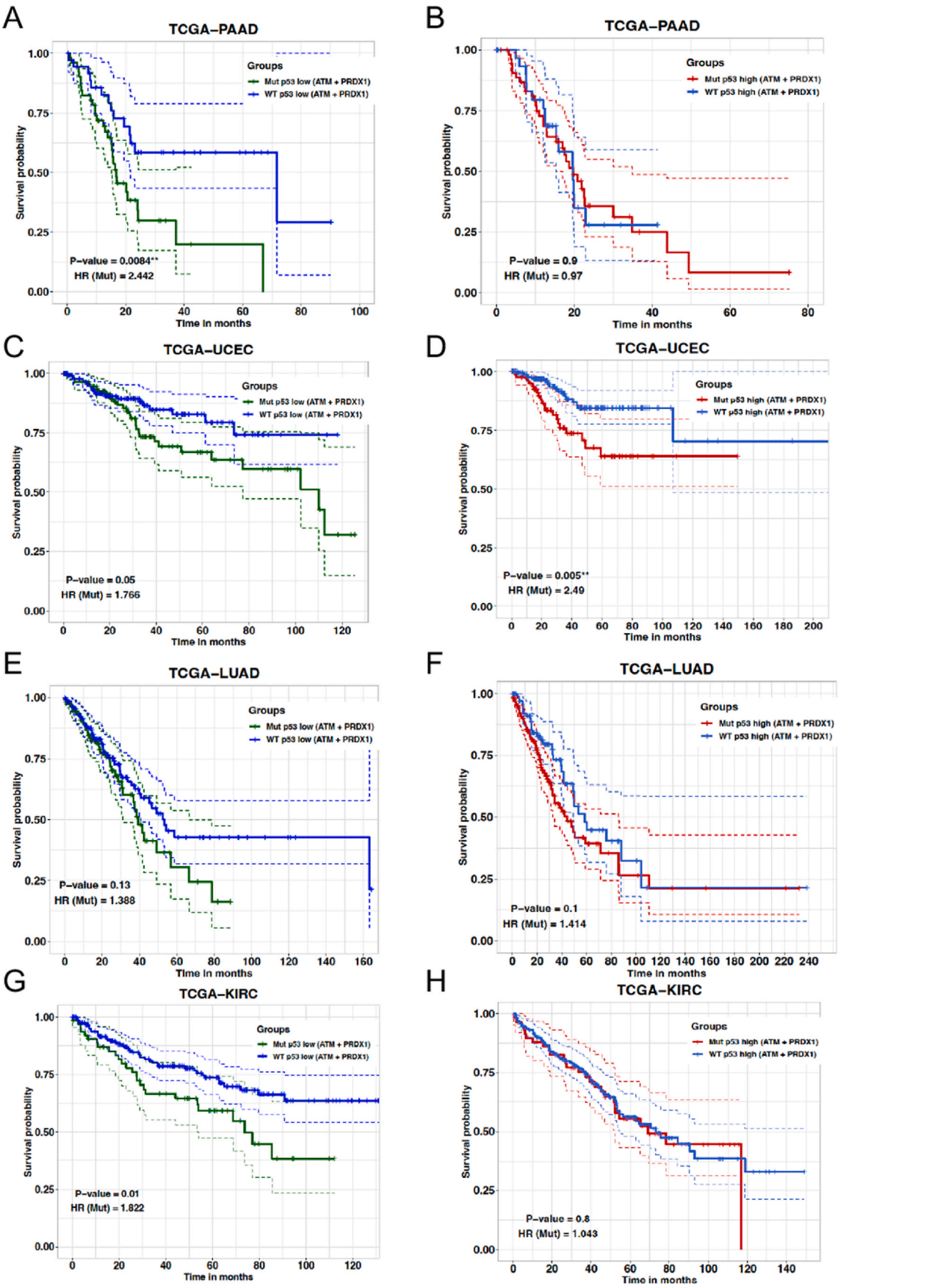

(caption on next page)

Fig. 6. p53 status dictates the survival of patients across multiple human malignancies when expression of ATM and PRDX1 is impaired.
(A, and B) Kaplan Meier (KM) survival curves of patients with pancreatic adenocarcinoma (PAAD). (A) Patients are stratified into two major groups, low expression of (ATM + PRDX1) genes with a wild type p53 status (WT p53) and low expression of (ATM + PRDX1) genes with a mutant p53 status (Mut p53). (B). A similar comparison was performed with patients with high expression of (ATM + PRDX1) genes. (C, and D) Kaplan Meier (KM) survival curves of patients with uterine corpus endometrial carcinoma (UCEC). A similar comparison between low and high (ATM + PRDX1) genes was performed as in (A, and B). (E, and F) Kaplan Meier (KM) survival curves of patients with lung adenocarcinoma (LUAD). A similar comparison between low and high (ATM + PRDX1) genes was performed as in (A, and B). (G, and H) Kaplan Meier (KM) survival curves of patients with kidney renal clear carcinoma (UCEC). A similar comparison between low and high (ATM + PRDX1) genes was performed as in (A, and B).

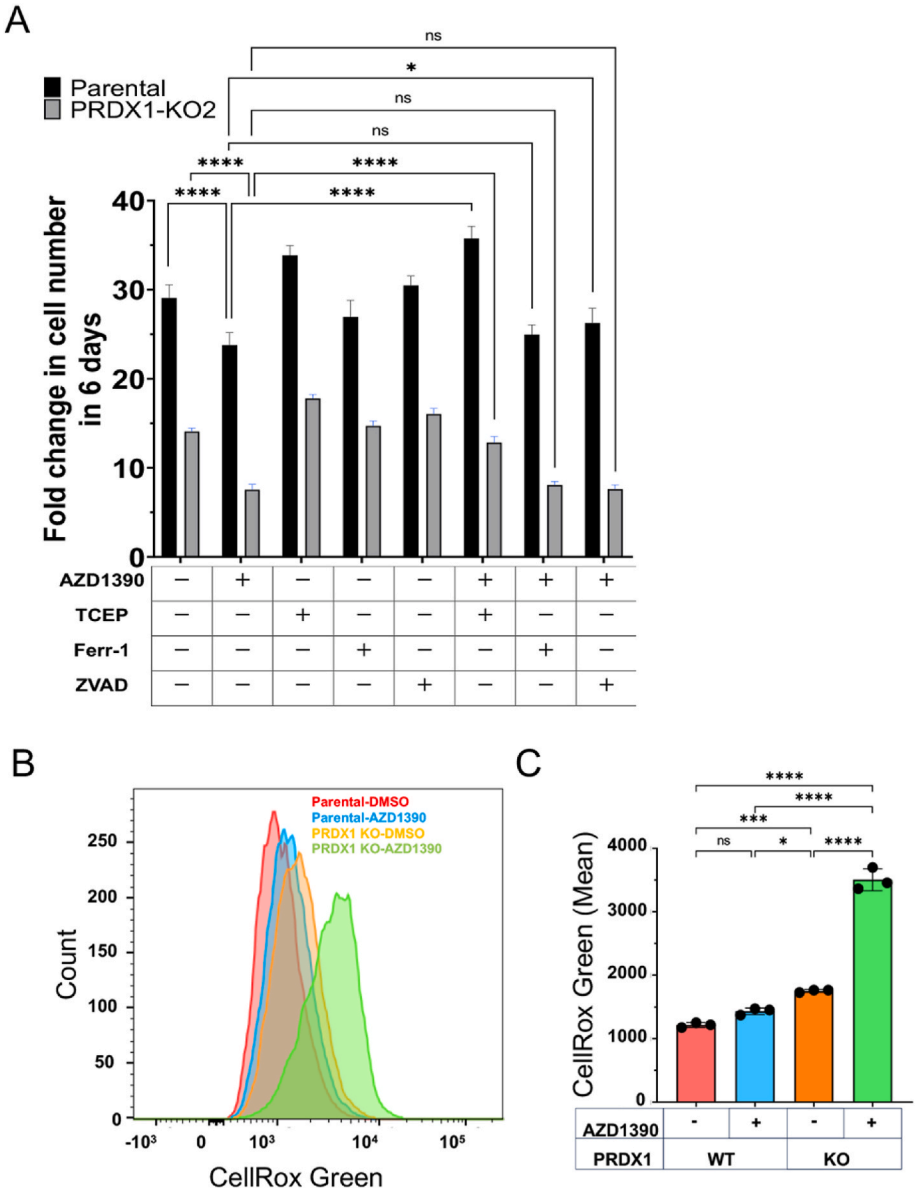

Fig. 7. ATM inhibition promotes disulfide stress in PRDX1-deficient cells. (A) Survival of A549 parental and PRDX1 knockout (KO) cells treated with AZD1390 (1 μM) for 6 days in the presence of agents mitigating cell death pathways such as disulfide stress (TCEP), ferroptosis (Ferrostatin-1), or apoptosis (Z-VAD). Data are represented as mean ± SD; $n = 4$. (B) Measurement of reactive oxygen species (ROS) in A549 parental and PRDX1 knockout (KO) cells treated with AZD1390 (1 μM) for 6 days employing *CellRox Green* in flow cytometry. (C) Quantification of reactive oxygen species (ROS) levels in panel B. Data are represented as mean ± SD; $n = 3$.

cells (green vs. blue in Fig. 7B–and C). These results indicated that PRDX1-deficient cells become more reliant on ATM for preventing ROS accumulation.

We hypothesized that ATM inhibition-induced disulfide stress upon PRDX1 loss may reflect a redox modification that includes a thiol-based oxidation or the formation of inter-and/or intramolecular disulfide bonds between the sulfhydryl groups of reactive cysteine residues in key redox-sensitive proteins responsible for p53 stabilization [21]. To test this hypothesis, we conducted a double alkylation assay to map the proteome-wide levels of free and oxidized cysteines in parental and PRDX1-deficient cells following ATM inhibitor treatment (Fig. 8A). Our analyses revealed over 2500 free cysteine and oxidized cysteine-containing proteins in approximately 3686 proteins. When normalized to total protein levels, only a fraction of proteins exhibited

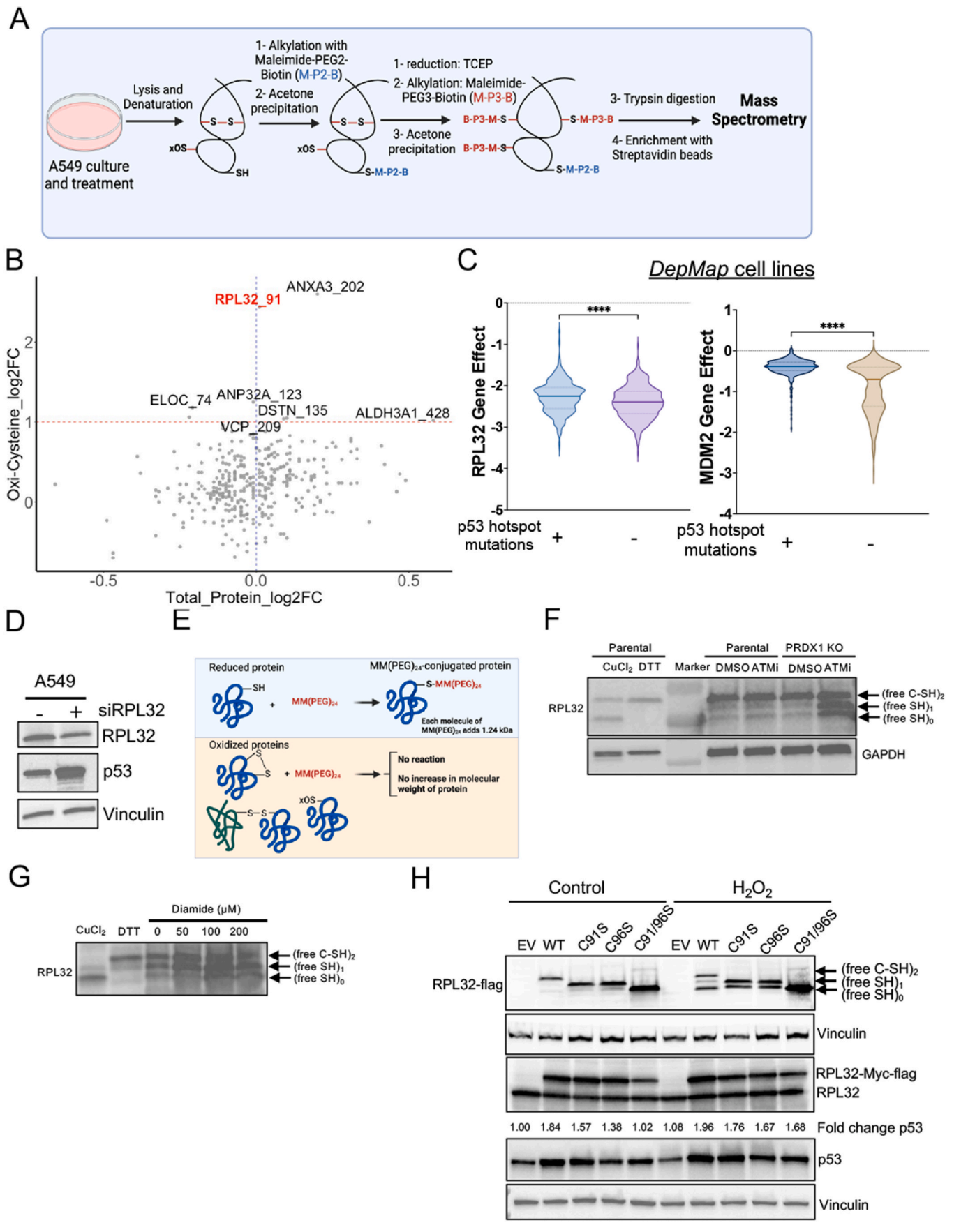

(caption on next page)

Fig. 8. RPL32 oxidation drives p53 stability. (A) Schematics of the Double alkylation approach employed to identify proteome-wide free thiols and disulfide-containing peptides. (B) Scatter plot of oxidized cysteine-containing peptides (dots) from the double alkylation assay as compared to total protein levels. Representative peptides labeled were upregulated at least 2-fold in PRDX1-knockout cells treated with AZD1390 in comparison to DMSO treatment. (C) Impact of RPL32 loss (left) and MDM2 loss (right) on cancer cells with/without p53 hotspot mutations. (D) Western blot of parental A549 cells transfected with siRNA targeting RPL32 for 48 h. (E) Schematics of $MM(PEG)_{24}$ conjugation-based approach to determine protein cysteine thiol redox status by western blot. (F) Cysteine thiol redox status in parental and PRDX1-knockout cells treated with AZD1390 (1 μM) or DMSO for 6 days. Parental cell lysate was incubated with $CuCl_2$ (30 μM) for the detection of oxidized RPL32, and with DTT (40 mM) for the detection of reduced RPL32. (G) Cysteine thiol redox status U2OS cells treated with the disulfide stress inducer diamide (200 μM) for 24 h. (H) Western blot of U2OS cells transfected with empty vector (EV), wild-type RPL32 (WT), C91S mutant form of RPL32 (C91S), C96S mutant form of RPL32 (C96S), or RPL32 double mutant (C91/96S) for 24 h. Cells were treated with hydrogen peroxide (H_2O_2 – 1mM) for 40 min. Vinculin was used as a loading control. $(Free\text{-}C\text{-}SH)_2$, $MM(PEG)_{24}$-conjugated RPL32 with two free cysteine residues; $(Free\text{-}C\text{-}SH)_1$, $MM(PEG)_{24}$-conjugated RPL32 with one free cysteine residue; $(Free\text{-}C\text{-}SH)_0$, $MM(PEG)_{24}$-unconjugated RPL32 with no free cysteine residue. Note. Fig. 8A is designed with *BioRender*.

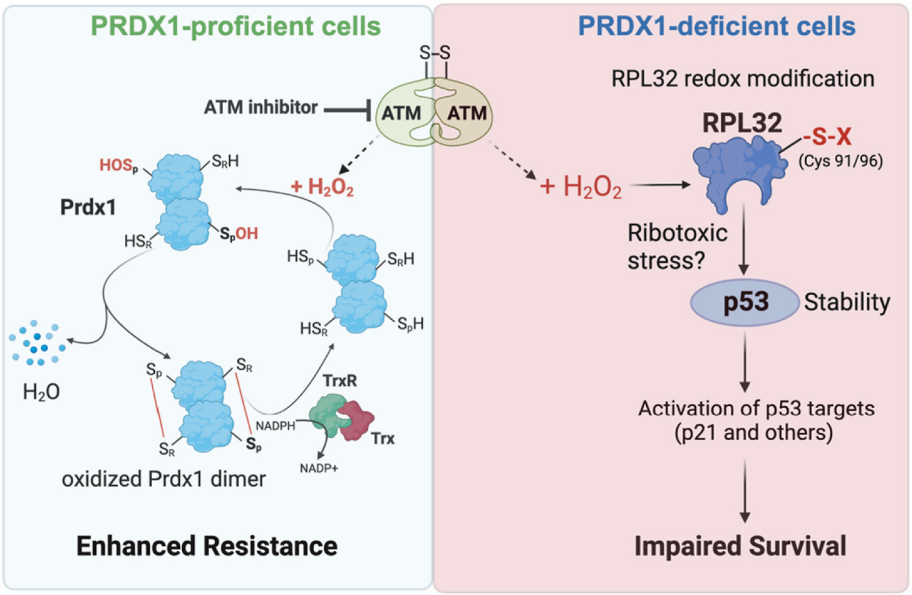

Fig. 9. Interplay between ATM and PRDX1 in tumor cells. This figure shows a simplified model depicting the role of PRDX1 loss, ATM inhibition, and RPL32 redox modification in p53 activation and cell survival. Note. This figure is designed with *BioRender*.

over a two-fold increase in oxidized cysteine-containing peptides (Fig. 8B). We identified the ribosomal protein RPL32 as the most abundant protein with a redox-modified cysteine (Cys-91) and unchanged protein level in PRDX1-knockout cells treated with the ATM inhibitor (Fig. 8B).

Ribosomal stress is well established to activate p53 and previous studies reported that RPL32 depletion is accompanied by p53 accumulation in NSCLCs, thus promoting cell death [44]. We employed the *DepMap* database to assess the degree to which RPL32 loss impacts the survival of wild-type and p53-mutated cells across various cancer cell lines. Our analysis revealed that RPL32 loss significantly impairs the growth of cancer cells with functional p53 while p53-mutated cells are more resistant to RPL32 loss (Fig. 8C, left panel), resembling the signature of MDM2, the master regulator of p53 stability (Fig. 8C, right panel). Consistently, silencing of RPL32 in A549 cells resulted in a significant accumulation of p53 levels (Fig. 8D).

We postulated that the oxidative stress resulting from ATM inhibition may promote RPL32 redox modification on Cys-91 inducing ribotoxic stress, thereby leading to the p53 activation. To validate this hypothesis, we utilized an $MM(PEG)_{24}$ conjugation-based approach to determine protein cysteine thiol redox status by western blotting [45] (Fig. 8E). The RPL32 protein contains 2 cysteine residues at positions 91 and 96. Consistent with the double alkylation results, ATM inhibition triggered RPL32 redox modification on Cysteine 91, but also on Cysteine 96, as evidenced by the presence of two $MM(PEG)_{24}$-conjugated RPL32 bands (Fig. 8F). Similar results were obtained upon treatment with diamide, a potent disulfide stress inducer (Fig. 8G).

To determine whether RPL32 redox modification is essential for p53 accumulation, we overexpressed the wild-type RPL32 and its mutant forms C91S, C96S, and C91/96S into U2OS cells, followed by exposure to oxidative stress with hydrogen peroxide treatment. The wild-type RPL32 promoted p53 accumulation (Fig. 8H), presumably due to an elevated change in the redox status of RPL32. In contrast, the overexpression of the RPL32-C91S and RPL32-C96S mutants and the RPL32-C91/96S double mutant led to a reduced accumulation of p53 (Fig. 8H). The apparent link between p53 levels and RPL32 redox status in untreated cells suggests that the endogenous ROS level may be sufficient to elicit significant changes in the redox status of RPL32. These observations suggest that RPL32 redox modification on Cysteine 91 and 96 is pivotal to p53 accumulation and may underlie the downstream activation of p53 in PRDX1-deficient cells, particularly upon ATM inhibition.

These findings collectively suggest that disulfide stress induced by ATM inhibition in PRDX1-deficient cells promotes RPL32 redox modification leading to p53 activation (Fig. 9). Future research is warranted to elucidate which specific redox modifications of RPL32 protein affect p53 stability, and if the redox status of RPL32 triggers ribotoxic stress to activate p53 signaling pathway.

While our results with TCEP treatment suggest that disulfide stress may be a key driver of cell death following ATM inhibition, previous research has highlighted a significant interplay between PRDX1 and p53. Notably, PRDX1 has been shown to act as an essential mediator for p53-induced apoptosis via MST1 kinase under conditions of high oxidative stress (46). This study unveiled a novel role for PRDX1 in regulating cell death in response to elevated oxidative stress, emphasizing the p53-dependent cytotoxic effects elicited by anticancer agents (46).

The significance of our findings lies in two major areas. First, we unveiled a novel synthetic lethal interaction between the inhibition of the ATM kinase, which plays significant roles in the DDR and redox metabolism, and deficiency in PRDX1, a protein known for its role in oxidants sensing and signaling pathways. This synthetic interaction is conserved across various cancer types, positioning PRDX1 as a universal synthetic lethality partner with ATM in tumors with functional p53. Second, we identify a new mode of p53 stability and activation mediated by disulfide stress upon ATM inhibition, findings which contrast with the canonical pathway of redox-dependent activation via ATM-driven p53 phosphorylation [37]. Our study suggests that stratifying patients with low *PRDX1* expression may help to identify responders to ATM inhibitors, based on the analysis of a large panel of human malignancies. While DDR inhibitors have shown promise in clinical use, their efficacy remains limited to a subset of cancer patients. By identifying new factors that influence the efficacy of DDR inhibitors, our study lays the groundwork for improving their use in a broader spectrum of cancers, benefiting a larger patient population. The identification of PRDX1 as a universal synthetic lethality partner with ATM marks a significant advancement in cancer therapeutics.

CRediT authorship contribution statement

Haojian Li: Writing – review & editing, Visualization, Validation, Formal analysis, Conceptualization. **Takashi Furusawa:** Writing – review & editing, Visualization, Validation, Formal analysis, Data curation. **Renzo Cavero:** Writing – review & editing, Visualization, Validation, Formal analysis. **Yunjie Xiao:** Validation, Formal analysis. **Raj Chari:** Resources, Data curation. **Xiaolin Wu:** Resources, Data curation. **David Sun:** Resources, Data curation. **Oliver Hartmann:** Writing – review & editing, Resources. **Anjali Dhall:** Writing – review & editing, Formal analysis. **Ronald Holewinski:** Methodology, Formal analysis. **Thorkell Andresson:** Writing – review & editing, Methodology, Formal analysis. **Baktiar Karim:** Formal analysis. **Marina Villamor-Payà:** Resources, Formal analysis. **Devorah Gallardo:** Methodology, Data curation. **Chi-Ping Day:** Writing – review & editing, Software, Resources, Conceptualization. **Lipika R. Pal:** Writing – review & editing, Software, Resources, Formal analysis. **Nishanth Ulhas Nair:** Writing – review & editing, Visualization, Software, Resources. **Eytan Ruppin:** Software, Resources. **Mirit I. Aladjem:** Writing – review & editing, Formal analysis. **Yves Pommier:** Writing – review & editing, Resources, Formal analysis. **Markus E. Diefenbacher:** Writing – review & editing, Resources, Methodology. **Jung Mi Lim:** Methodology, Resources. **Rodney L. Levine:** Methodology, Resources. **Travis H. Stracker:** Writing – review & editing, Resources. **Urbain Weyemi:** Writing – review & editing, Writing – original draft, Supervision, Resources, Project administration, Methodology, Investigation, Funding acquisition, Formal analysis, Conceptualization.

Declaration of competing interest

The authors declare that they have no known competing financial interests or personal relationships that could have appeared to influence the work reported in this paper.

Acknowledgments

We thank the CCR Genomics Core for help with the RNA-seq experiments. We also thank Dr. William M. Bonner (Emeritus Scientist, NCI), Dr. Kandice Tanner, and Dr. Myriem Boufraqech of the National Cancer Institute, for their thoughtful critiques and their help with reviewing this manuscript. We thank *AstraZeneca* for kindly providing AZD0156 compound. We are indebted to Ian Riekhof for help with the experiments. This work is supported by the NCI Center for Cancer Research (CCR) and has been funded in whole or in part with Federal funds from the National Cancer Institute, National Institutes of Health. D.S., X.W., R.C., R.H., T.A., and B.K., were supported by National Cancer Institute under contract no. 75N91019D00024. The content of this publication does not necessarily reflect the views or policies of the Department of Health and Human Services, nor does mention of trade names, commercial products, or organizations imply endorsement by the U.S. Government. The authors thank Yolanda L. Jones, NIH Library Editing Service, for editing assistance. O.H. and M.E.D. are funded by the DKH 70112013 and DIP DI 931/18-1 DIP.

Appendix A. Supplementary data

Supplementary data to this article can be found online at https://doi.org/10.1016/j.redox.2025.103503.

Data availability

The accession number for the datasets reported in this paper (RNA-seq (A549-Cas9 and NCI–H1299)) are GEO: GSE272107 at https://www.ncbi.nlm.nih.gov/geo/query/acc.cgi?acc=GSE272107. The computer code generated during the current study is available on reasonable request.

References

[1] A. Tubbs, A. Nussenzweig, Endogenous DNA damage as a source of genomic instability in cancer, Cell 168 (2017) 644–656.
[2] A.N. Blackford, S.P. Jackson, ATM, ATR, and DNA-PK: the trinity at the heart of the DNA damage response, Mol. Cell 66 (2017) 801–817.
[3] Y. Shiloh, Y. Ziv, The ATM protein kinase: regulating the cellular response to genotoxic stress, and more, Nat. Rev. Mol. Cell Biol. 14 (2013) 197–210.
[4] J.H. Lee, T.T. Paull, Cellular functions of the protein kinase ATM and their relevance to human disease, Nat. Rev. Mol. Cell Biol. 22 (2021) 796–814.
[5] M. Choi, T. Kipps, R. Kurzrock, ATM mutations in cancer: therapeutic implications, Mol. Cancer Therapeut. 15 (2016) 1781–1791.
[6] P.G. Pilie, C. Tang, G.B. Mills, T.A. Yap, State-of-the-art strategies for targeting the DNA damage response in cancer, Nat. Rev. Clin. Oncol. 16 (2019) 81–104.
[7] T.T. Paull, Mechanisms of ATM activation, Annu. Rev. Biochem. 84 (2015) 711–738.
[8] S.T. Durant, et al., The brain-penetrant clinical ATM inhibitor AZD1390 radiosensitizes and improves survival of preclinical brain tumor models, Sci. Adv. 4 (2018) eaat1719.
[9] H. Li, et al., CRISPR metabolic screen identifies ATM and KEAP1 as targetable genetic vulnerabilities in solid tumors, Proc. Natl. Acad. Sci. U. S. A. 120 (2023) e2212072120.
[10] G. Rotman, Y. Shiloh, Ataxia-telangiectasia: is ATM a sensor of oxidative damage and stress? Bioessays 19 (1997) 911–917.
[11] Z. Guo, S. Kozlov, M.F. Lavin, M.D. Person, T.T. Paull, ATM activation by oxidative stress, Science 330 (2010) 517–521.
[12] Y. Zhang, et al., Mitochondrial redox sensing by the kinase ATM maintains cellular antioxidant capacity, Sci. Signal. 11 (2018).
[13] J.H. Lee, T.T. Paull, Mitochondria at the crossroads of ATM-mediated stress signaling and regulation of reactive oxygen species, Redox Biol. 32 (2020) 101511.
[14] C. Cosentino, D. Grieco, V. Costanzo, ATM activates the pentose phosphate pathway promoting anti-oxidant defence and DNA repair, EMBO J. 30 (2011) 546–555.
[15] E.F. Fang, et al., NAD(+) replenishment improves lifespan and healthspan in ataxia telangiectasia models via mitophagy and DNA repair, Cell Metabol. 24 (2016) 566–581.
[16] H.M. Chow, et al., ATM is activated by ATP depletion and modulates mitochondrial function through NRF1, J. Cell Biol. 218 (2019) 909–928.
[17] K. Birsoy, et al., An essential role of the mitochondrial electron transport chain in cell proliferation is to enable aspartate synthesis, Cell 162 (2015) 540–551.
[18] B. Wang, et al., Integrative analysis of pooled CRISPR genetic screens using MAGeCKFlute, Nat. Protoc. 14 (2019) 756–780.
[19] N. McCabe, et al., Mechanistic rationale to target PTEN-deficient tumor cells with inhibitors of the DNA damage response kinase ATM, Cancer Res. 75 (2015) 2159–2165.
[20] T. Fischer, et al., PTEN mutant non-small cell lung cancer require ATM to suppress pro-apoptotic signalling and evade radiotherapy, Cell Biosci. 12 (2022) 50.
[21] C.A. Neumann, J. Cao, Y. Manevich, Peroxiredoxin 1 and its role in cell signaling, Cell Cycle 8 (2009) 4072–4078.
[22] S.G. Rhee, H.A. Woo, D. Kang, The role of peroxiredoxins in the transduction of H (2)O(2) signals, Antioxidants Redox Signal. 28 (2018) 537–557.
[23] J.J. Skoko, et al., Redox regulation of RAD51 Cys319 and homologous recombination by peroxiredoxin 1, Redox Biol. 56 (2022) 102443.
[24] C.C. Winterbourn, M.B. Hampton, Thiol chemistry and specificity in redox signaling, Free Radic. Biol. Med. 45 (2008) 549–561.
[25] C.C. Winterbourn, Hydrogen peroxide reactivity and specificity in thiol-based cell signalling, Biochem. Soc. Trans. 48 (2020) 745–754.

[26] S. Stocker, M. Maurer, T. Ruppert, T.P. Dick, A role for 2-Cys peroxiredoxins in facilitating cytosolic protein thiol oxidation, Nat. Chem. Biol. 14 (2018) 148–155.
[27] M.C. Sobotta, et al., Peroxiredoxin-2 and STAT3 form a redox relay for H2O2 signaling, Nat. Chem. Biol. 11 (2015) 64–70.
[28] H.Z. Chae, S.J. Chung, S.G. Rhee, Thioredoxin-dependent peroxide reductase from yeast, J. Biol. Chem. 269 (1994) 27670–27678.
[29] S.W. Kang, et al., Mammalian peroxiredoxin isoforms can reduce hydrogen peroxide generated in response to growth factors and tumor necrosis factor-alpha, J. Biol. Chem. 273 (1998) 6297–6302.
[30] H.Z. Chae, T.B. Uhm, S.G. Rhee, Dimerization of thiol-specific antioxidant and the essential role of cysteine 47, Proc. Natl. Acad. Sci. U. S. A. 91 (1994) 7022–7026.
[31] B.L. Hopkins, et al., A peroxidase peroxiredoxin 1-specific redox regulation of the novel FOXO3 microRNA target let-7, Antioxidants Redox Signal. 28 (2018) 62–77.
[32] J. Cao, et al., Prdx1 inhibits tumorigenesis via regulating PTEN/AKT activity, EMBO J. 28 (2009) 1505–1517.
[33] M. Olahova, et al., A redox-sensitive peroxiredoxin that is important for longevity has tissue- and stress-specific roles in stress resistance, Proc. Natl. Acad. Sci. U. S. A. 105 (2008) 19839–19844.
[34] J.S. Lee, et al., Synthetic lethality-mediated precision oncology via the tumor transcriptome, Cell 184 (2021) 2487–2502.
[35] G.S. Cowley, et al., Parallel genome-scale loss of function screens in 216 cancer cell lines for the identification of context-specific genetic dependencies, Sci. Data 1 (2014) 140035.
[36] H.W. Cheung, et al., Systematic investigation of genetic vulnerabilities across cancer cell lines reveals lineage-specific dependencies in ovarian cancer, Proc. Natl. Acad. Sci. U. S. A. 108 (2011) 12372–12377.
[37] C. Cirotti, et al., Redox activation of ATM enhances GSNOR translation to sustain mitophagy and tolerance to oxidative stress, EMBO Rep. 22 (2021) e50500.
[38] W.T. Chen, et al., ATM regulation of IL-8 links oxidative stress to cancer cell migration and invasion, Elife 4 (2015).
[39] M. Haj, et al., Accelerated replicative senescence of ataxia-telangiectasia skin fibroblasts is retained at physiologic oxygen levels, with unique and common transcriptional patterns, Aging Cell 22 (2023) e13869.
[40] E. Aeby, W. Ahmed, S. Redon, V. Simanis, J. Lingner, Peroxiredoxin 1 protects telomeres from oxidative damage and preserves telomeric DNA for extension by telomerase, Cell Rep. 17 (2016) 3107–3114.
[41] A. Moretton, et al., A metabolic map of the DNA damage response identifies PRDX1 in the control of nuclear ROS scavenging and aspartate availability, Mol. Syst. Biol. 19 (2023) e11267.
[42] L. Cao, et al., ATM-Chk2-p53 activation prevents tumorigenesis at an expense of organ homeostasis upon Brca1 deficiency, EMBO J. 25 (2006) 2167–2177.
[43] O. Hartmann, et al., Implementation of CRISPR/Cas9 genome editing to generate murine lung cancer models that depict the mutational landscape of human disease, Front. Cell Dev. Biol. 9 (2021) 641618.
[44] J. Xie, et al., RPL32 promotes lung cancer progression by facilitating p53 degradation, Mol. Ther. Nucleic Acids 21 (2020) 75–85.
[45] B.D. Pant, S. Oh, K.S. Mysore, Protocol for determining protein cysteine thiol redox status using western blot analysis, STAR Protoc 2 (2021) 100566.